RSC Advances

PAPER

View Article Online
View Journal | View Issue

Check for updates

Cite this: *RSC Adv.*, 2022, **12**, 8719

Pomegranate seed polyphenol-based nanosheets as an efficient inhibitor of amyloid fibril assembly and cytotoxicity of HEWL†

Ali Akbar Meratan, *[a] Vahid Hassani,[a] Atiyeh Mahdavi[a] and Nasser Nikfarjam [b]

Poor water solubility and low bioavailability are considered as two main factors restricting therapeutic applications of natural polyphenols in relation to various disorders including amyloid-related diseases. Among various strategies developed to overcome these limitations, nanonization has attracted considerable attention. Herein, we compared the potency of bulk and nano forms of the polyphenolic fraction of pomegranate seed (PFPS) for modulating Hen Egg White Lysozyme (HEWL) amyloid fibril formation. Prepared PFPS nanosheets using direct oxidative pyrolysis were characterized by employing a range of spectroscopic and microscopic techniques. We found that the nano form can inhibit the assembly process and disintegrate preformed fibrils of HEWL much more effective than the bulk form of PFPS. Moreover, MTT-based cell viability and hemolysis assays showed the capacity of both bulk and nano forms of PFPS in attenuating HEWL amyloid fibril-induced toxicity, where the nano form was more effective. On the basis of thioflavin T results, a delay in the initiation of amyloid fibril assembly of HEWL appears to be the mechanism of action of PFPS nanosheets. We suggest that the improved efficiency of PFPS nanosheets in modulating the HEWL fibrillation process may be attributed to their increased surface area in accord with the surface-assistance model. Our results may present polyphenol-based nanosheets as a powerful approach for drug design against amyloid-related diseases.

Received 31st July 2021
Accepted 9th March 2022

DOI: 10.1039/d1ra05820g

rsc.li/rsc-advances

Open Access Article. Published on 21 March 2022. Downloaded on 6/3/2026 11:06:32 PM.
This article is licensed under a Creative Commons Attribution-NonCommercial 3.0 Unported Licence.

Introduction

Among approaches developed for amyloid fibrillation inhibition, use of naturally-occurring molecules, especially certain dietary polyphenols, has attracted a great attention.[1] However, there are a number of challenges that limit development of natural polyphenols as therapeutic agents relating to amyloid-related diseases. These include poor water solubility and stability, low absorption upon oral administration, and rapid metabolism under physiological conditions. Moreover, because of their hydrophobic nature, most of polyphenols are not expected to cross the blood–brain barrier (BBB), where they may demonstrate their neuroprotective effects.[2,3] In recent years, nanonization, the process of size reduction of particles to nanoscale, especially with a sheet-like structure,[4,5] has become one of the interesting research topics. In the case of polyphenols, nanonization has been considered as a promising approach to increase water solubility and bioavailability, and improve the pharmacological effects of these compounds.[6–8] Interestingly, many recent reports show that nanoformulation of various natural polyphenols significantly improves their affinity for amyloidogenic species as well as their capacity to bypass tissue filtration and cross the BBB, where they effectively influence amyloid fibril formation and even target amyloid plaques.[9–13] Pomegranate (*Punica granatum* L.) is an ancient edible fruit with a very diverse chemical composition including flavonoids, polyphenols, minerals, fatty acids, tannins, anthocyanins, and complex carbohydrates.[14] It has been reported that extracts from different parts of pomegranate exhibit therapeutic properties and target a wide range of diseases including various types of cancer, cardiovascular diseases,[15] diabetes,[16] AIDS, obesity, and neurodegenerative disorders.[17] These activities are mostly considered to be related to ellagitannins (including punicalagins), and various classes of polyphenolic compounds such as flavonoids, anthocyanidins, anthocyanins, flavonols, and flavones.[17] Although several mechanisms are suggested to be related to the therapeutic benefits of pomegranate, it's antioxidant, anticarcinogenic, and anti-inflammatory properties have attracted the most attention.[17] Regarding to the neurodegenerative diseases, some investigators have found that pomegranate extracts/constituents could be used as a novel protectant.[18–26] However, poor water solubility, low bioavailability, and inability to cross BBB are the main challenges restricting their therapeutic applications, leading to attempts to solve these problems.[27,28] Recently, we reported that

[a]*Department of Biological Sciences, Institute for Advanced Studies in Basic Sciences (IASBS), Zanjan 45137-66731, Iran. E-mail: a.meratan@iasbs.ac.ir*

[b]*Department of Chemistry, Institute for Advanced Studies in Basic Sciences (IASBS), Zanjan 45137-66731, Iran*

† Electronic supplementary information (ESI) available. See DOI: 10.1039/d1ra05820g

© 2022 The Author(s). Published by the Royal Society of Chemistry

Open Access Article. Published on 21 March 2022. Downloaded on 6/3/2026 11:06:32 PM.
This article is licensed under a Creative Commons Attribution-NonCommercial 3.0 Unported Licence.

polyphenolic fraction of propolis, in the nanosheet form, exhibits an improved capacity for modulating the assembly process as well as clearance of preformed fibrils of bovine insulin, and concluded that increased water solubility and surface area upon nanosheet formation might be involved.[29] This finding suggests that nanoformulation of polyphenolic compounds, naturally occurring in fruits and plants, could be a promising approach for drug design relating to the neurological disorders. To further confirm this proposition, self-polymerization of the polyphenolic fraction of pomegranate seed (PFPS) was performed through direct pyrolysis. The bulk and nano forms of PFPS (PFPS nanosheets) were structurally and morphologically characterized. This was followed by employing a range of amyloid-specific techniques to compare the efficacy of bulk and nano forms of PFPS in modulating hen egg white lysozyme (HEWL) amyloid fibrillation process. HEWL is one of the most extensively studied proteins which assemble into amyloid fibrils under *in vitro* conditions.[30] Moreover, structural homology with human lysozyme, which it's amyloid deposits are related to systemic amyloidosis,[31] has made HEWL an attractive model for *in vitro* fibrillation studies. Obtained results clearly demonstrated that PFPS nanosheets, compared to their respective bulk form, were much more effective in inhibiting HEWL amyloid fibrillation and clearance of preformed fibrils, indicating improved anti-amyloidogenic properties of PFPS in the nano form.

Materials and methods

Materials

HEWL, Thioflavin T (ThT), Congo red (CR), Nile red (NR), 3-(4,5-dimethyl tiazol-2-yl)-2,5 diphenyl tetrazolium bromide (MTT), and dialysis tube were purchased from Sigma (St. Louis, MO, USA). SH-SY5Y cells were a gift from Dr Karima (Shahid Beheshti University of Medical Sciences, Tehran, Iran). The cell culture medium (DMEM-F12), fetal bovine serum (FBS), and penicillin–streptomycin antibiotics were purchased from Gibco BRL (Life Technology, Paisley, Scotland). *n*-Hexane was purchased from CARLO ERBA, France. All other chemicals were obtained from Merck (Darmstadt, Germany) and were reagent grade.

Extraction of polyphenolic fraction of pomegranate seed (PFPS)

Pomegranates were collected from the Mazandaran, Iran. Fifty grams of the dried pomegranate seeds were grinded finely, and then it's fatty acid content was extracted with Soxhlet using *n*-hexane for 24 h. To extract PFPS, the resultant powder was dried and then dispersed in 100 mL of deionized water (DW), stirred for 24 h, and filtered on a Whatman filter paper to eliminate non-soluble materials. Finally, the suspension was evaporated in an oven at 60 °C, and the resultant brown powder (Fig. S1A†) was grinded finely and stored in a dark place for subsequent experiments.

Preparation of PFPS nanosheets

PFPS nanosheets were prepared using direct oxidative pyrolysis, as previously reported with slight modifications.[29] Briefly, one gram of the PFPS powder was added into a 10 mL beaker and heated to 200 °C for 2.5 min. A color change from brown to dark brown indicates successful pyrolysis and nanosheet formation. Then, the sample was quickly neutralized by adding 200 mL of 250 mM NaOH and stirred at room temperature (RT) for 8 h. The obtained suspension was filtered on a Whatman filter paper and dialyzed (using cut-off 12 kDa dialysis tube) against DW until neutral pH was achieved. The resultant dialyzed solution, containing the purified PFPS nanosheets, was dried in an oven at 60 °C. Finally, the obtained dark brown powder (Fig. S1B†) was grinded finely and stored in a dark place for subsequent experiments.

Characterization of bulk and nano forms of PFPS

Nanonization progress was confirmed by UV-Vis, FT-IR, and X-ray photoelectron spectroscopies. The UV-Vis spectrum of bulk and nano forms of PFPS (20 μg mL^{-1}) was recorded using a spectrophotometer (UV-2550, Shimadzu). For FT-IR spectroscopy, samples were dried in a vacuum oven at 60 °C. The related spectrums were obtained from 400 to 4000 cm^{-1} using a Bruker spectrometer (EQUINOX 55 Bruker, Germany) by preparing their KBr pellets. X-ray photoelectron spectroscopy (XPS) analysis was performed using a K-alpha X-ray photoelectron spectrometer. The fluorescence emission spectra of bulk and nano forms of PFPS were measured in aqueous solution (10 μg mL^{-1}) by a fluorescence spectrophotometer (Cary Eclipse VARIAN, Mulgrave, Australia) with a slit width of 5 nm for both excitation and emission. The thermal stability of bulk and nano forms of PFPS was determined by a thermal gravimetric analyzer (NETZSCH STA 409 PC/PG). The samples were dried in a vacuum oven at 60 °C and thermal gravimetric analysis (TGA) was performed as described.[29] The surface zeta potential of PFPS nanosheets (20 μg mL^{-1}) in a range of pH (from 2 to 12) was recorded using a zeta potential analyzer (Brookhaven Instrument, Holtsville, NY 11742-1896, USA). Finally, the microscopic features of PFPS nanosheets were analyzed using electron and atomic force microscopies. Briefly, aliquots of an aqueous suspension of PFPS nanosheets (~20 μg mL^{-1}) were placed on a carbon-coated copper grid and dried at RT. The samples were analyzed using a Philips CM300 transmission electron microscope (TEM). An aliquot of aqueous suspension was dropped on a clean glass slide and dried in the oven at 60 °C, coated with a gold layer and imaged by the field emission scanning electron microscopy (FE-SEM, Hitachi S4160 operating at 20 kV). Finally, for atomic force microscopy (AFM), aliquots of PFPS nanosheets solution (diluted with DW to a final concentration of 15 μg mL^{-1}) were placed on a freshly cleaved mica and dried at RT. Images were acquired as reported previously.[29]

Sample preparation

Protein sample was dissolved in 50 mM glycine buffer (pH 2.2) in a final concentration of 7.5 mg mL^{-1} (~500 μM). The stock

© 2022 The Author(s). Published by the Royal Society of Chemistry

Open Access Article. Published on 21 March 2022. Downloaded on 6/3/2026 11:06:32 PM.
This article is licensed under a Creative Commons Attribution-NonCommercial 3.0 Unported Licence.

solutions of bulk and nano forms of PFPS were prepared at 5 and 100 mg mL^{-1}, respectively, using DW as solvent, and were stored at −20 °C until use (Fig. S1C†). The molar ratios of bulk/nano forms of PFPS to the HEWL used in this study were 1 : 150, 1 : 50, and 1 : 33.

HEWL amyloid fibril formation and characterization

For amyloid fibrillation induction, aliquots of HEWL, containing 20 μM thioflavin T (ThT) and various concentrations (0, 50, 150, and 225 μg mL^{-1}) of bulk or nano forms of PFPS, were transferred into a non-binding black surface with clear bottom polystyrene 96-well plate (Corning Incorporated, 2 Alfred Road, Kennebunk ME 04043 USA) with a final volume of 200 μL of assay solution in each well. The plate was sealed with crystal clear sealing tape (Axygen, Corning Incorporated USA) and loaded into a Synergy Hybrid Multi-Mode microplate reader (BioTek Instruments, Winooski, VT 05404-0998, USA) followed by incubation at 57 °C without agitation. The fluorescence signal was measured at 10 h intervals, with excitation at 440 nm and emission at 485 nm for 8 days. In all experiments, ThT fluorescence measurement was done in triplicate and the mean of the three measurements was determined. The acquired data from ThT fluorescence measurements were fitted to the sigmoid curve and kinetics parameters were determined according to the equation described by Nielsen *et al.*[32] For Nile red (NR) fluorescence measurements, aliquots of protein solutions were removed at the end of incubation time and diluted to a final concentration of 5 μM, using H_2O containing 50 μM NR. Samples were excited at 530 nm and emission spectra were recorded from 550–800 nm. For Congo red (CR) binding assay, aliquots of incubated HEWL (final concentration of 5 μM), were added to 950 μL of CR solution (20 μM). After 30 min of incubation at RT, absorbance spectra were recorded between 400 and 600 nm. The amount of bound CR was quantified according to the equation described by Klunk *et al.*[33] Far-UV CD spectra were recorded in the range of 190–260 nm using an AVIV 215 spectropolarimeter (Aviv Associates, Lakewood, NJ, USA), in a final concentration of 30 μM in glycine buffer (50 mM, pH 2.2). Finally, 10 μL of the incubated samples (diluted to a final concentration of 25 μM) were mixed with 10 μL of ThT solution (100 μM) and incubated for 10 min in a dark place at RT. The mixture was added on a clean glass slide and air-dried. The images were captured on a fluorescence microscope (Zeiss, Germany) at 20× magnification.

SDS-PAGE analysis

Sodium dodecyl sulfate-polyacrylamide gel electrophoresis (SDS-PAGE) was performed without boiling treatment. Aliquots (20 μL) corresponding to HEWL incubated under amyloidogenic conditions for 8 days, either alone or in the presence of various concentrations of bulk or nano forms of PFPS, were mixed with 10 μL of the sample buffer and applied onto the gel (15%). Electrophoresis was performed at constant voltage at 100 V. Gel was stained with 0.025% (w/v) Coomassie brilliant blue followed by multiple destaining.

Remodeling activity of bulk and nano forms of PFPS

Matured fibrils of HEWL were prepared by incubation of the protein solutions under amyloidogenic conditions for sufficient time, as described before. Then, aliquots (200 μL) of preformed amyloid fibrils were incubated alone or with various concentrations of bulk or nano forms of PFPS (150, 300, and 600 μg mL^{-1}) at 37 °C for 96 h. The disaggregating potency of bulk and nano forms of PFPS was investigated by ThT assay and fluorescence microscopy imaging as described above.

In vitro cell viability assay

Human neuroblastoma SH-SY5Y cells, were cultured in DMEM-F12 medium as reported previously.[34] For cytotoxicity experiments, cells were treated with increasing amounts (0–2000 μg mL^{-1}) of bulk or nano forms of PFPS, or HEWL amyloid fibrils (0–50 μM) and incubated for 24 h. To evaluate the protective effects of bulk/nano forms of PFPS against toxicity induced by HEWL amyloid fibrils, the aliquots of incubated samples, aged without or with various concentrations of bulk/nano forms of PFPS under amyloidogenic conditions, were added to the cells (in a final concentration of 20 μM) and left for 24 h. Cells treated with 50 mM glycine buffer (pH 2.2) were used as control. Cell viability was assessed using the conventional MTT reduction assay. Results were expressed as percentage of MTT reduction relative to the control cells, assuming that the absorbance of control cells was 100%.

In vitro hemolysis assay

The hemolytic activity of bulk/nano forms of PFPS (0–400 μg mL^{-1}), or HEWL amyloid fibrils (0–50 μM) was evaluated as described previously.[29] To evaluate the protective effects of bulk/nano forms of PFPS against permeabilization induced by HEWL amyloid fibrils, the cell suspensions (1% hematocrit) were incubated alone or with various concentrations of incubated samples for 3 h at 37 °C while being gently stirred. The samples were then centrifuged at 1000 g for 10 min, followed by measuring the absorbance of supernatants at 540 nm. The percentage of hemolysis was calculated as a fraction of the maximum effect (1% (v/v) Triton X-100): (measured signal-blank signal)/(maximum signal-blank signal). For microscopy imaging, 10 μL of resultant pellets (diluted 3 fold with phosphate buffered saline) were added on a clean glass slide and air-dried. The images were captured on an optical microscope (Nikon, Japan) at 20× magnification.

Statistical analysis

All assays were performed two or three times with triplicate repeats. Data are expressed as percentage of values in untreated control cells, and each value represents the mean ± SD ($n = 3$). The significant differences between the means of the treated and untreated groups were calculated by unpaired Student's *t*-test and *p*-values less than 0.01 were considered significant. $*p < 0.01$, $**p < 0.001$ were significantly different from control cells/erythrocytes. $^{\#}p < 0.01$ was significantly different from those exposed only to HEWL amyloid fibrils.

Open Access Article. Published on 21 March 2022. Downloaded on 6/3/2026 11:06:32 PM.
This article is licensed under a Creative Commons Attribution-NonCommercial 3.0 Unported Licence.

Results and discussion

Extraction of PFPS, synthesis and characterization of PFPS nanosheets

The high fatty acid content of pomegranate seed was first removed by Soxhlet using *n*-hexane as solvent. It's polyphenolic content was then extracted by DW as described above. Indeed, this simple method provides an efficient way to extract the relative hydrophilic polyphenols of pomegranate seed, with the aim to prepare final hydrophilic water-soluble nanosheets. Combustion, pyrolysis, oxidative coupling, carbonization and hydrothermal carbonization are well-known methods to obtain value-added products from naturally-occurring polyphenols. However, due to existence of various polyphenols, in different content and chemical structure, investigating the mechanism of reactions occurring in these processes have many challenges.[35] The PFPS nanosheets were fabricated through the pyrolysis process in the presence of atmospheric oxygen, leading to the fusion of polyphenolic species by reacting oxygen-containing functional groups like hydroxyl and carboxyl groups and forming the related ether and ester bridges. It worth to note that, decarboxylation of compounds and decomposition of ester-containing polyphenols during the process would diminish the possibility of polyphenols self-condensation.[36] But, that's not the whole story, the phenoxy radicals formed in polyphenols structure show a resonance in which the radical character is localized on the *ortho*- and *para*-carbons as well as the phenolic oxygen, which can lead to self-condensation of polyphenols *via* the C–O and C–C bonds.[37] The charge densities calculations have revealed that 41.3% and 39.1% of the spin densities are located on the phenolic and *para*-carbons, respectively,[38] indicating that the polyphenols are mostly self-condensed through these two sites. The UV-Vis absorption spectrum of bulk form of PFPS showed a maximum absorption peak at 283 nm (corresponding to the typical π–π* transition of C=C) with a shoulder at about 350 nm (corresponding to the *n*–π* transition of C=O bond) (Fig. 1A), indicating the presence of flavonoids/polyphenols.[39,40] Upon undergoing nanonization, however, we observed a significant enhancement in the absorption spectrum with a blue shift (Fig. 1A). Despite confinement of the chromophore regions (*i.e.*, short ranged ordered sp^2 domains) by atoms with sp^3 hybridization, it seems that the number of these regions is increased, likely due to the fusion of polyphenolic compounds during the nanonization process, leading to increased UV-Vis absorption of PFPS nanosheets (Fig. 1A). One notable characteristic of the bulk and nano forms of PFPS is their excitation wavelength-dependent emission. While the bulk form of PFPS shows some fluorescence properties (Fig. S2†), we observed a considerable emission for PFPS nanosheets (Fig. 1B). This may be attributed to the

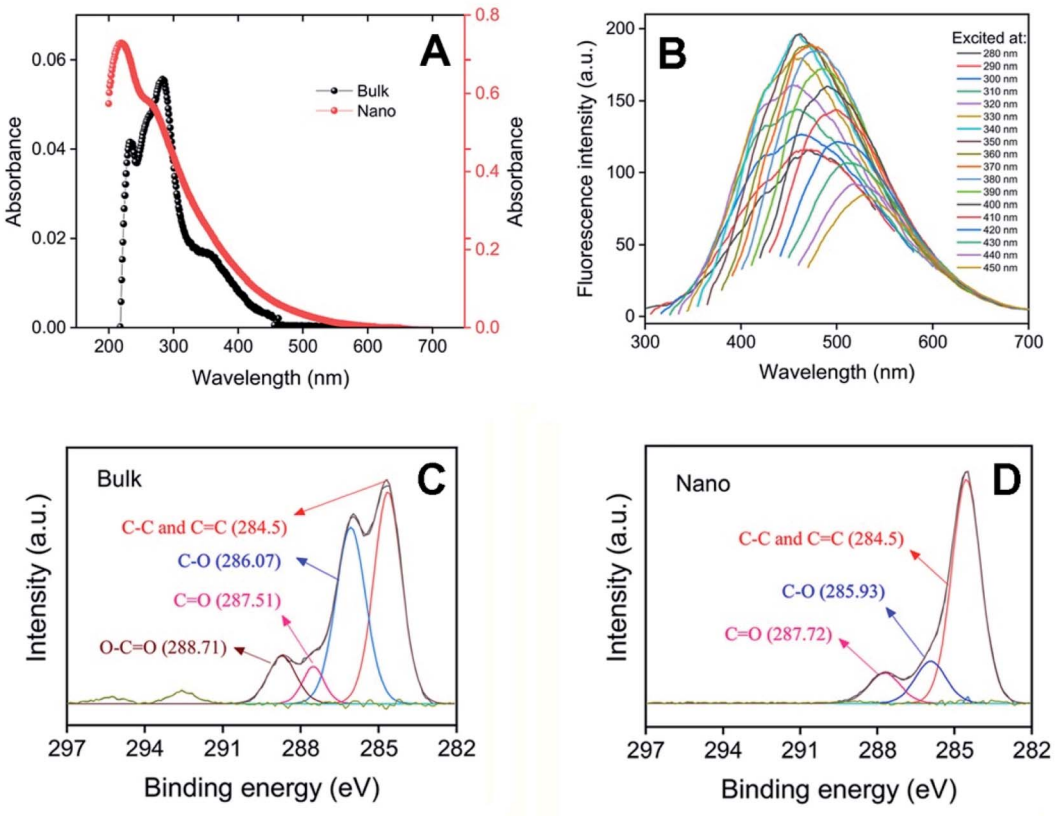

Fig. 1 Spectroscopic characterization of bulk and nano forms of PFPS. (A) UV-Vis absorption spectra of bulk (left axis) and nano (right axis) forms of PFPS (20 μg mL^{-1} aqueous solutions). (B) Fluorescence emission spectra of PFPS nanosheets, excited at different wavelengths. (C and D) C 1s spectra of bulk and nano forms of PFPS, respectively.

© 2022 The Author(s). Published by the Royal Society of Chemistry

Open Access Article. Published on 21 March 2022. Downloaded on 6/3/2026 11:06:32 PM.
This article is licensed under a Creative Commons Attribution-NonCommercial 3.0 Unported Licence.

increased number of chromophore regions as described above, leading to a significant fluorescence with various emission patterns (Fig. 1B and S3†), a sign of non-uniformity in the size of chromophore regions in the PFPS nanosheets.[41] As shown in Fig. 1B, the maximum emission of PFPS nanosheets is around 460 nm when excited at 350 nm. The emission peak shifts to shorter wavelengths (up to excitation at 320 nm) and longer wavelengths (up to excitation at 450 nm). The shift is more obvious when the fluorescence intensity is normalized at different excitation wavelengths (Fig. S3†). This excitation wavelength-dependent emission property of nano form is due to the inhomogeneity of the particle sizes and plenteous emissive traps of surface states formed by the hydroxy, carboxy and other oxygen-based functional groups.[42,43] We believe that the prepared nanostructures have non-directional nature due to C–C cross linking phenolic moieties of polyphenols. Consequently, the configuration of interconnected carbon network would be tilted or rotated leading to isotopically bundled three-dimensional architectures. This would generate a non-graphitized phase of hard carbon with abundant structural defects after pyrolysis. Therefore, these structural defects along with those derived from partially carbonization can lead to short-range-ordered sp^2-carbon domains of hard carbons. Moreover, due to the complicated mixture of polyphenols, it seems that there are various ordered sp^2-carbon domains of different sizes which can result in excitation wavelength-dependent emission. We believe that the fluorescence property of PFPS nanosheets may provide these structures with the potential to use as imaging probes for protein aggregates detection. The FT-IR spectroscopy was employed to determine the functional groups in bulk and nano forms of PFPS. For the bulk form, the characteristic peaks are 3000–3200 (aromatic C–H), 2850–2925 (aliphatic C–H), 1475, 1531, and 1600 (aromatic C=C), 1730 (C=O of ester and/or aldehyde groups), 1664 (ketone group), 1027, 1070, and 1232 cm^{-1} (C–O) (Fig. S4†). The assigned peak sequences at 690–900 cm^{-1} are for "out of plane"' (oop) bending, indicating aromatic ring substitutes.[29] Upon undergoing nanonization, the spectrum pattern was changed due to the fusion of polyphenolic molecules and the production of a new structure. As shown in Fig. S4,† broad peaks at 1554–1760 (aromatic C=C and C=O), 1000–1200 (C–O), and 3600 cm^{-1} (O–H) indicate the fundamental structural changes in the polyphenolic structures leading to the formation of various oxygen-based functional groups in the course of nanonization process.[29] These structural changes were further confirmed by XPS analysis. The C 1s spectrum of bulk form was deconvoluted into four peaks including 284.5 eV (aromatic and aliphatic C=C), 286.07 eV (C–O), 287.51 eV (C=O), and 288.71 eV (O–C=O) (Fig. 1C). Upon nanonization, however, the C 1s spectrum of PFPS nanosheets was deconvoluted into three peaks including 284.5 eV (aromatic and aliphatic C=C), 285.93 eV (C–O), and 287.72 eV (C=O) (Fig. 1D).[29,44–46] Comparison of the XPS spectrums and extracted data revealed a decrement in the intensity of C–O and C=O peaks, and disappearance of the O–C=O peak as well, upon nanonization (Fig. 1C, D and Table 1). Thus, the high abundance of C=C, compared to C–O and C=O, groups may provide another reason for the notable fluorescence properties of PFPS nanosheets (Fig. 1B and S3†). These observations suggest that PFPS molecules can be fused and combined by eliminating oxygen-containing small molecules such as water and alcohol. Moreover, it seems that the carboxylic groups in PFPS nanosheets undergo decarboxylation and produce CO_2 during the pyrolysis process. As depicted in Fig. S5,† the surface zeta potential of PFPS nanosheets follows a pH-dependent decrease from +1.14 to −22.99 and then increased to −14.77 mV, indicating an isoelectric point around 1.7. In almost the whole pH range, the negative surface charge may be related to deprotonation of various functional groups existing in the structure of PFPS nanosheets.[29] The increased of zeta potential by changing pH from 7.3 to 11.5 is likely related to the ion screening effect.[47,48] The TEM and AFM images revealed around and sheet morphology with a diameter ranging from 400 to 600 nm and an average thickness of 2–3 nm (Fig. 2). The formation of stacked nanosheets may suggest the involvement of both lateral and vertical hydrogen bonds, mediated by the presence of oxygen-based functional groups. The FE-SEM images were also confirmed their potential to aggregate while drying (Fig. S6†). The thermal stability of the bulk and nano forms of PFPS was studied by TGA. Four main weight losses at temperatures below 100 °C (elimination of physically adsorbed water), between 130–250 °C and 250–367 °C (likely due to removal of flavonoids/polyphenols), and above 500 °C (probably due to the decomposition of resistant aromatic structures of biogenic salts such as carbonates[29,49]), was observed for the bulk form of PFPS (Fig. 3). In the case of nano form, we observed three main weight losses (Fig. 3). The first one below 100 °C relating to the elimination of physically adsorbed water. The second one ranging from 206–480 °C, is more likely due to the removal of functional groups, existing on the surface of PFPS nanosheets,

Table 1 Obtained data from XPS analysis of C 1s in bulk and nano forms of PFPS

	Bulk				Nano			
Bond type	Peak energy bond, eV	Height ratio	Area ratio	FWHM, eV	Peak energy bond, eV	Height ratio	Area ratio	FWHM, eV
C=C, C–C	284.64	1	1	1.32	284.55	1	1	1.38
C–O	286.07	0.83	0.89	1.41	285.93	0.19	0.2	1.45
C=O	287.51	0.18	0.13	1.01	287.72	0.14	0.15	1.47
O–C=O	288.71	0.23	0.23	1.32	—	—	—	—

Open Access Article. Published on 21 March 2022. Downloaded on 6/3/2026 11:06:32 PM.
This article is licensed under a Creative Commons Attribution-NonCommercial 3.0 Unported Licence.

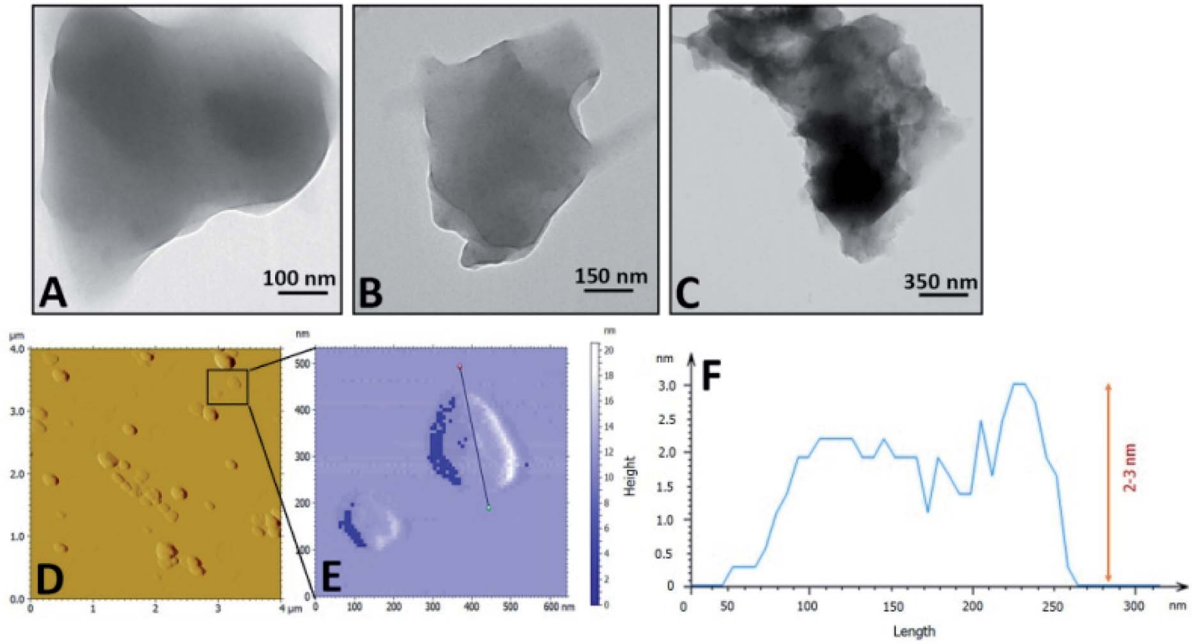

Fig. 2 Microscopic characterization of PFPS nanosheets. (A–C) TEM images; and (D and E) AFM imagesand (F) related line profile of PFPS nanosheets, respectively.

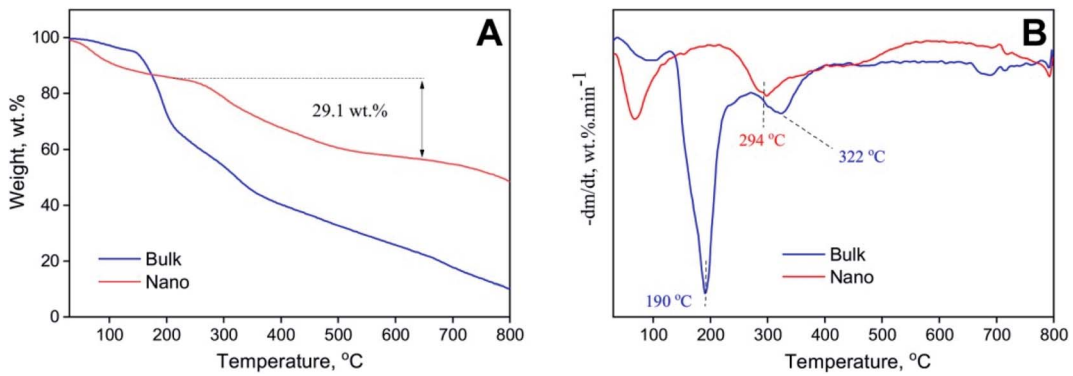

Fig. 3 Thermal stability of bulk and nano forms of PFPS. (A) TGA; and (B) DTG thermograms of bulk and nano forms of PFPS.

and physically adsorbed organic polyphenols, accounting for 29.10 wt% or, in other words 34.03 wt% of the total weight of PFPS nanosheets (Fig. 3). The third weight loss observed above 660 °C may attribute to the decomposition of main skeleton of PFPS nanosheets. TGA results suggest increased thermal stability of PFPS nanosheets, especially at high temperatures.

Effect of bulk and nano forms of PFPS on fibrillation process of HEWL

ThT fluorescence assay was employed to monitor the effect of bulk and nano forms of PFPS on the amyloid fibril formation of HEWL. From data depicted in Fig. 4A and B, it can clearly conclude that PFPS, in either bulk and nano forms, can modulate HEWL fibrillation process dose-dependently. However, at a same concentration, nano form of PFPS was found much more effective. As shown in Fig. 4A, in the presence of various concentrations of bulk form a dose-dependent decrease in ThT fluorescence intensity, with some increase in the nucleation phase duration (Table 2), was observed. In samples treated with nano form of PFPS, however, decrease in ThT fluorescence intensity was accompanied with a more significant elongation of the nucleation phase, as in the presence of 225 μg mL^{-1} PFPS nanosheets the fibrillation process of HEWL was completely inhibited without any detectible lag time (Fig. 4B and Table 2). These results suggest that PFPS, in the nanosheet form, exhibits enhanced capacity to delay and inhibit amyloid fibril assembly of HEWL. This improved efficiency of PFPS nanosheets was further confirmed by CR binding assay (Fig. S7†). The higher anti-amyloidogenic properties of PFPS nanosheets, compared to its respective bulk form, were further confirmed by fluorescence microscopy and SDS-PAGE analysis. The morphology of structures produced alone or in the presence of increasing concentrations of bulk/nano forms of PFPS were examined by fluorescence microscopy. As shown in Fig. 4C, incubation of protein samples for 8 days under amyloidogenic condition is

© 2022 The Author(s). Published by the Royal Society of Chemistry

Open Access Article. Published on 21 March 2022. Downloaded on 6/3/2026 11:06:32 PM.
This article is licensed under a Creative Commons Attribution-NonCommercial 3.0 Unported Licence.

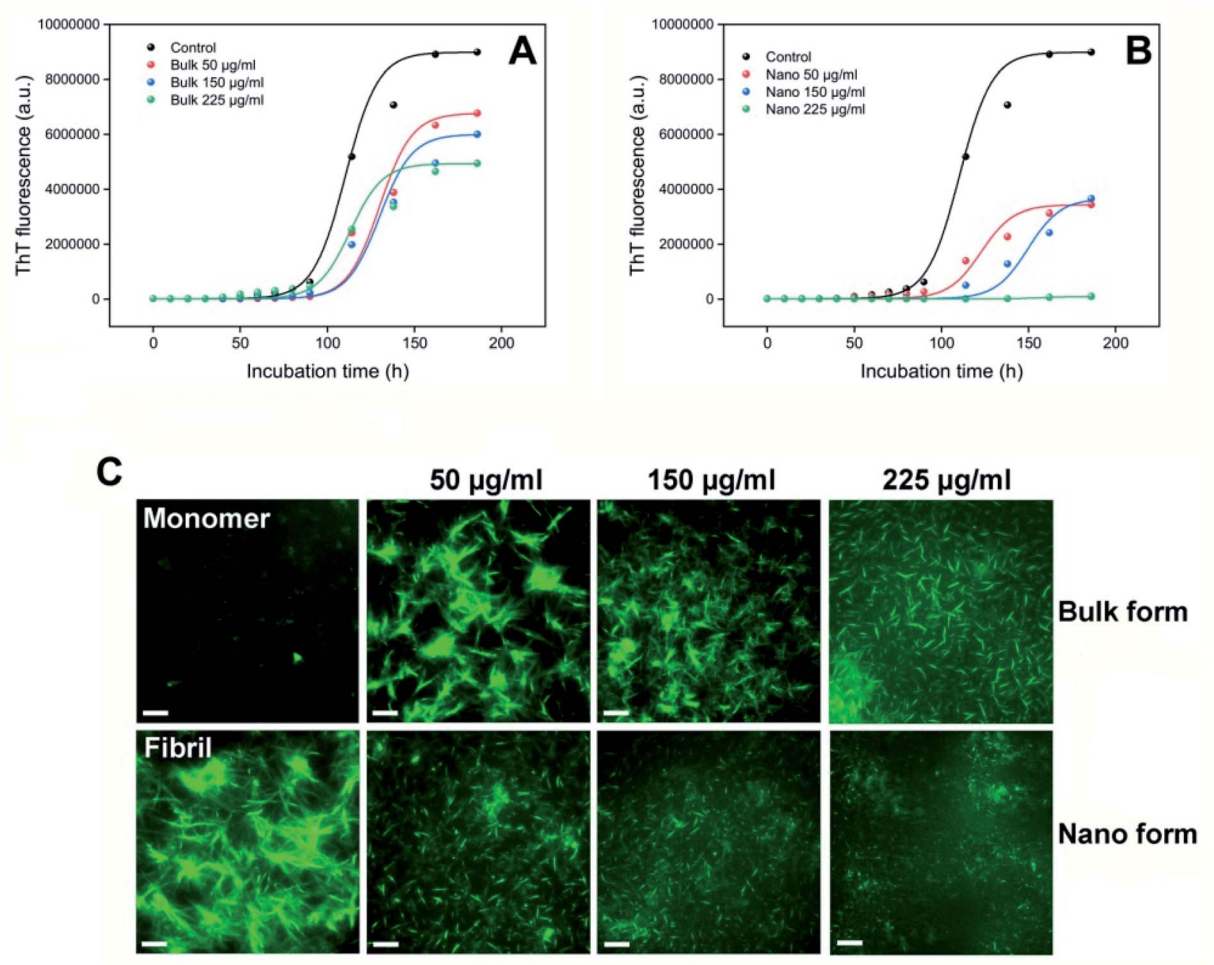

Fig. 4 Effect of bulk and nano forms of PFPS on amyloid fibrillation of HEWL. (A and B) Kinetics of HEWL amyloid fibril formation monitored by increasing fluorescence intensity of ThT at 485 nm. (C) Fluorescence microscopy images of HEWL samples incubated without or with various concentrations of the bulk or nano forms of PFPS for 8 days. The scale bars represent 500 nm.

Table 2 Effect of bulk and nano forms of PFPS on the kinetics parameters of HEWL amyloid fibrillation

	Lag time (h)	t_{50} (h)	Amplitude $\times 10^{-3}$
Control	79.44 ± 1.81	110.88 ± 1.34	8990 ± 272.88
Bulk 50 μg mL^{-1}	101.89 ± 3.29	130.07 ± 3.91	6770 ± 77.88
Bulk 150 μg mL^{-1}	102.92 ± 1.50	128.21 ± 3.31	6000 ± 92.73
Bulk 225 μg mL^{-1}	90.12 ± 2.10	113.55 ± 1.19	4940 ± 71.18
Nano 50 μg mL^{-1}	102.11 ± 1.63	122.61 ± 1.15	3430 ± 43.20
Nano 150 μg mL^{-1}	128.51 ± 3.00	148.61 ± 2.03	3660 ± 77.88
Nano 225 μg mL^{-1}	—[a]	165.1 ± 2.88	95.94 ± 1.49

[a] The lag time could not be determined in the presence of 225 μg mL^{-1} nano form of PFPS since aggregation was not observed.

sufficient to induce the formation of mature amyloid fibrils. The presence of bulk form of PFPS caused a dose-dependent inhibition of amyloid fibrils formation (Fig. 4C). In samples containing 225 μg mL^{-1} bulk form of PFPS, the formation of such fibrillar structures was prominently prevented, with the appearance of short amyloid fibrils (Fig. 4C). In samples treated with PFPS nanosheets, however, the extent of inhibition was more effective, as in samples containing 225 μg mL^{-1} PFPS nanosheets, no detectible structure was seen (Fig. 4C). The SDS-PAGE profile of incubated samples is depicted in Fig. 5. For the protein samples incubated alone a band trapped in the well of stacking gel, corresponding to high molecular weight amyloid fibrils, was seen. The presence of either bulk or nano forms of PFPS, however, caused a dose-dependent transition from large aggregates into low molecular weight intermediates and monomeric species; where nanosheets were more effective (Fig. 5). This observation further confirms the higher efficiency of nano form of PFPS to delay the initiation of HEWL fibrillation process, in accord with ThT fluorescence results (Fig. 4A and B). On the basis of obtained results, we suggest that in the presence of high concentrations of PFPS nanosheets, formation of mature fibrils is strongly inhibited. These results are in accord with our recent report,[29] suggesting that nano form of polyphenolic compounds, in comparison with their respective bulk form, may exhibit improved capacity to modulate the assembly process of various amyloidogenic peptides and proteins. The size-dependent modulating effect of PFPS on HEWL

Open Access Article. Published on 21 March 2022. Downloaded on 6/3/2026 11:06:32 PM.
This article is licensed under a Creative Commons Attribution-NonCommercial 3.0 Unported Licence.

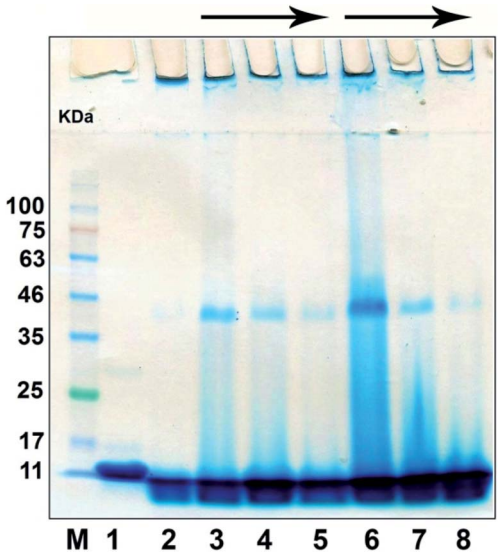

Fig. 5 SDS-PAGE analysis of HEWL samples incubated alone or with increasing concentrations of the bulk or nano forms of PFPS for 8 days. The lanes represent native HEWL (lane 1), samples incubated alone (lane 2) or with various concentrations of bulk (lanes 3–5) or nano (lanes 6–8) forms of PFPS. The arrows indicate the increasing concentration of the bulk/nano forms of PFPS corresponding to 50, 150, or 225 μg mL^{-1}. Left lane represents protein marker.

fibrillation process is in accord with the surface-assistance model, reported by other studies.[50–52] While the bulk form of PFPS was somewhat water-soluble (up to 5 mg mL^{-1}), upon nanosheet formation, we were able to prepare a 100 mg mL^{-1} aqueous solution of PFPS. Clearly, this improved water solubility would increase capacity of PFPS nanosheets for hydrogen bonding/electrostatic interactions with surrounding molecules including HEWL monomers. This can lead to more efficient interaction with HEWL monomers of nano, compared to bulk, form of PFPS. Additionally, we suggest that increased surface area as well as chemical modifications introduced upon nanonization may also be involved. On the other hand, due to increased surface area, PFPS nanosheets exhibit a significantly high protein absorption capacity. Accordingly, nano form of PFPS may deplete a large fraction of monomers form the solution leading to decreased solution concentration and aggregation rate of the protein.[50]

Effect of bulk and nano forms of PFPS on structural/conformational changes of HEWL

In continuous of the study, the structural/conformational changes of HEWL in the absence and presence of bulk and nano forms of PFPS were examined using far-UV CD and NR fluorescence experiments. As depicted in Fig. 6, incubation of HEWL alone under amyloidogenic conditions caused

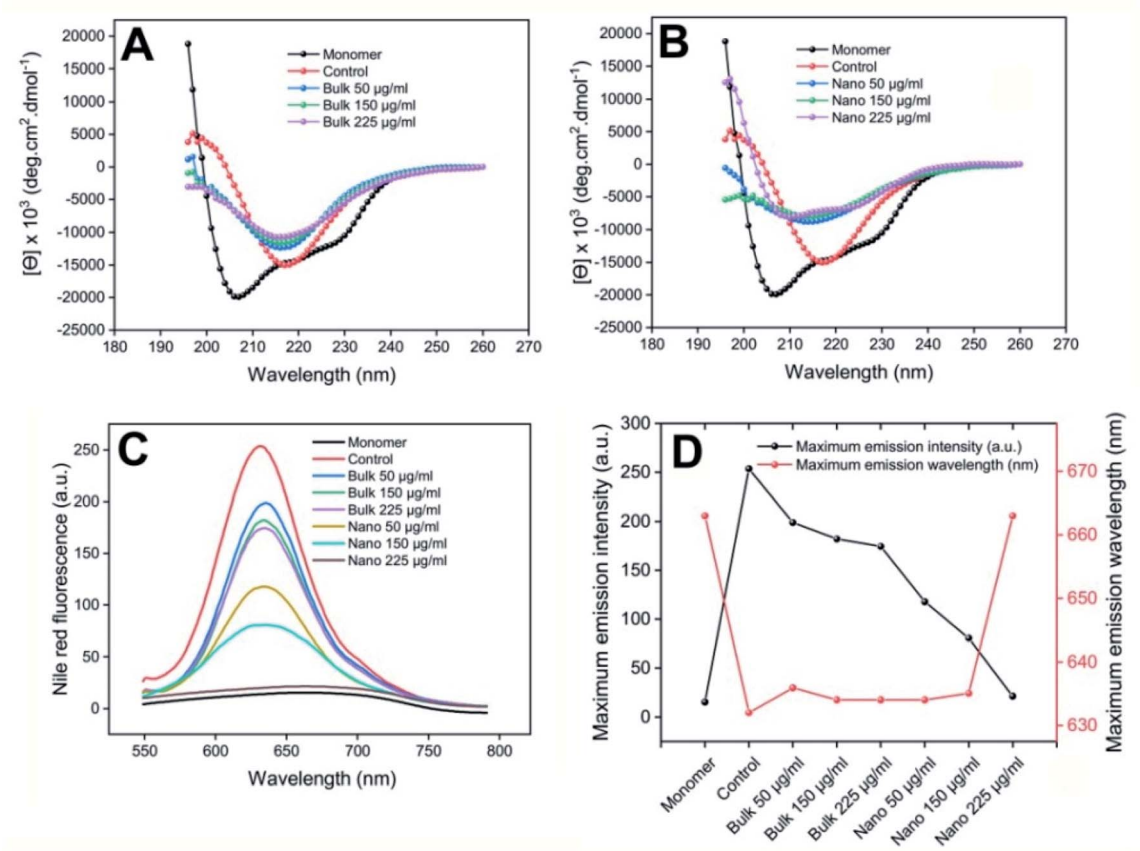

Fig. 6 Effect of bulk and nano forms of PFPS on structural/conformational changes of HEWL. (A and B) Far-UV CD spectra of HEWL samples incubated with the bulk or nano forms of PFPS, respectively. (C) Changes in surface hydrophobicity of HEWL samples incubated with the bulk or nano forms of PFPS, respectively, as measured by NR fluorescence assay. (D) Left-hand and right-hand y axes show maximum emission intensity and maximum emission wavelength of incubated samples, respectively. Further descriptions are provided in the text.

© 2022 The Author(s). Published by the Royal Society of Chemistry

Open Access Article. Published on 21 March 2022. Downloaded on 6/3/2026 11:06:32 PM.
This article is licensed under a Creative Commons Attribution-NonCommercial 3.0 Unported Licence.

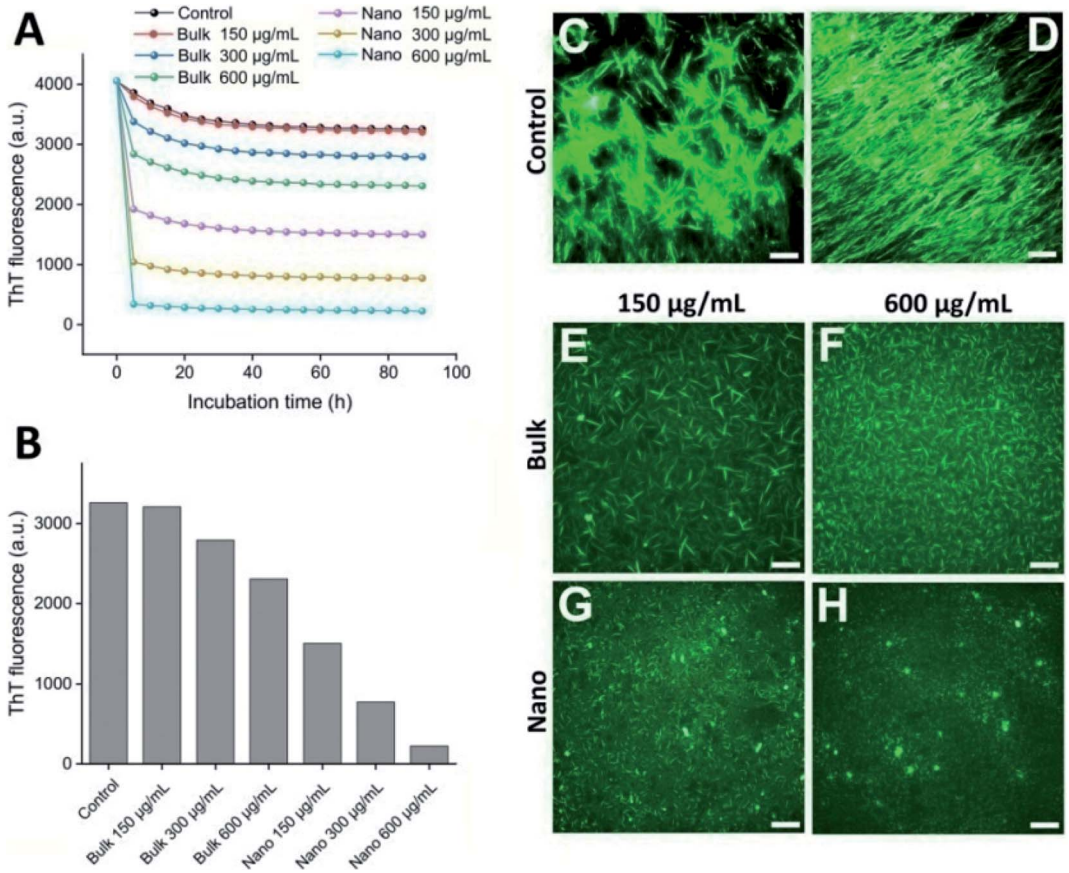

Fig. 7 Remodeling of preformed fibrils of HEWL by bulk or nano forms of PFPS. (A) Remodeling kinetics of preformed fibrils of HEWL demonstrated by decreasing fluorescence intensity of ThT at 485 nm. (B) An enlarged view of the changes in the fluorescence emission intensity of incubated samples after 1.5 h incubation. (C–H) Fluorescence microscopy images of preformed fibrils of HEWL before (C) or after incubation at 37 °C either alone (D) or with 150 (E) or 600 (F) μg mL^{-1} bulk, or 150 (G) or 600 (H) μg mL^{-1} nano forms of PFPS for 96 h. The scale bars represent 500 nm.

significant conformational changes characterized by a gradual transition from a predominant α-helix to a β-sheet structure and a considerable enhancement in NR fluorescence signal with a pronounced blue shift of the spectrum from 663 nm to 632 nm. However, the presence of either bulk or nano forms of PFPS prevented such structural/conformational changes; where PFPS nanosheets showed more efficiency (Fig. 6). It worth to note that, although secondary structural transitions caused by amyloidogenic conditions were not completely inhibited in the presence of neither bulk nor nano forms of PFPS (Fig. 6A and B), we observed an effective suppression of the exposure of hydrophobic regions, along with a considerable red shift, in the samples incubated with 225 μg mL^{-1} PFPS nanosheets (Fig. 6C and D). This observation indicates that the presence of PFPS nanosheets has resulted in prevention of solvent-exposure of hydrophobic regions.

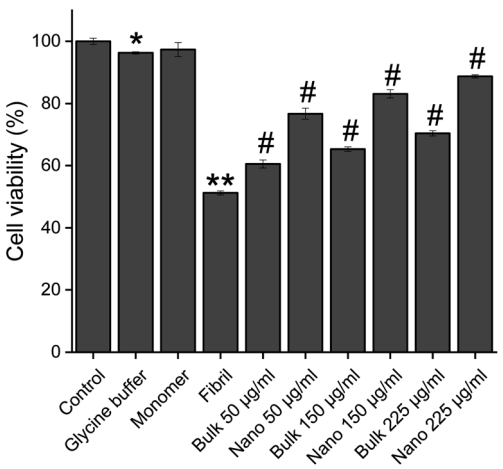

Fig. 8 Effect of the bulk and nano forms of PFPS on cytotoxicity induced by HEWL aggregates. Further descriptions are provided in the text. *$p < 0.01$, **$p < 0.001$, significantly different from control cells. #$p < 0.001$, significantly different from cells exposed only to HEWL amyloid fibrils.

Remodeling activity of bulk and nano forms of PFPS

The potency of bulk and nano forms of PFPS to disaggregate preformed fibrils of HEWL was investigated by ThT assay and fluorescence microscopy imaging. As illustrated in Fig. 7A, the both bulk and nano forms of PFPS were able to disaggregate

Open Access Article. Published on 21 March 2022. Downloaded on 6/3/2026 11:06:32 PM.
This article is licensed under a Creative Commons Attribution-NonCommercial 3.0 Unported Licence.

preformed fibrils of HEWL in a dose-dependent manner. Interestingly, decrease in fluorescence intensity of ThT was very fast, reaching a maximum decrement during the first few hours of incubation (Fig. 7A and B). However, with the same concentration, nano form of PFPS can more efficiently disaggregate the amyloid fibrils (Fig. 7A and B). For instance, the performance of 150 μg mL^{-1} nano form is better than 600 μg mL^{-1} bulk form of PFPS (Fig. 7A and B). As shown in Fig. 7D, further incubation of HEWL fibrils at 37 °C led to generation of very long fibrils assembled in large bundles, indicating the continuation of amyloid fibril assembly. While disintegration of the HEWL fibrils mediated by either bulk or nano forms of PFPS was considerable, nanosheets were more effective (Fig. 7E–H). As illustrated in Fig. 7H, in the presence of 600 μg mL^{-1} PFPS nanosheets we almost observed complete disintegration of amyloid fibrils without any detectable fibrillar structure. Through bearing a larger surface area, we speculate that *via* broad interaction and binding to fibrillar aggregates, PFPS nanosheets may disintegrate fibrillar structures more effective that the bulk form of PFPS, further clarifying surface-assistance model.[50–52] Moreover, modification of surface functional groups upon nanonization, evidenced by various spectroscopic measurements, may also involve in facilitating absorption of fibrillar aggregates at the surface of PFPS nanosheets. However, further studies are needed to validate this proposition.

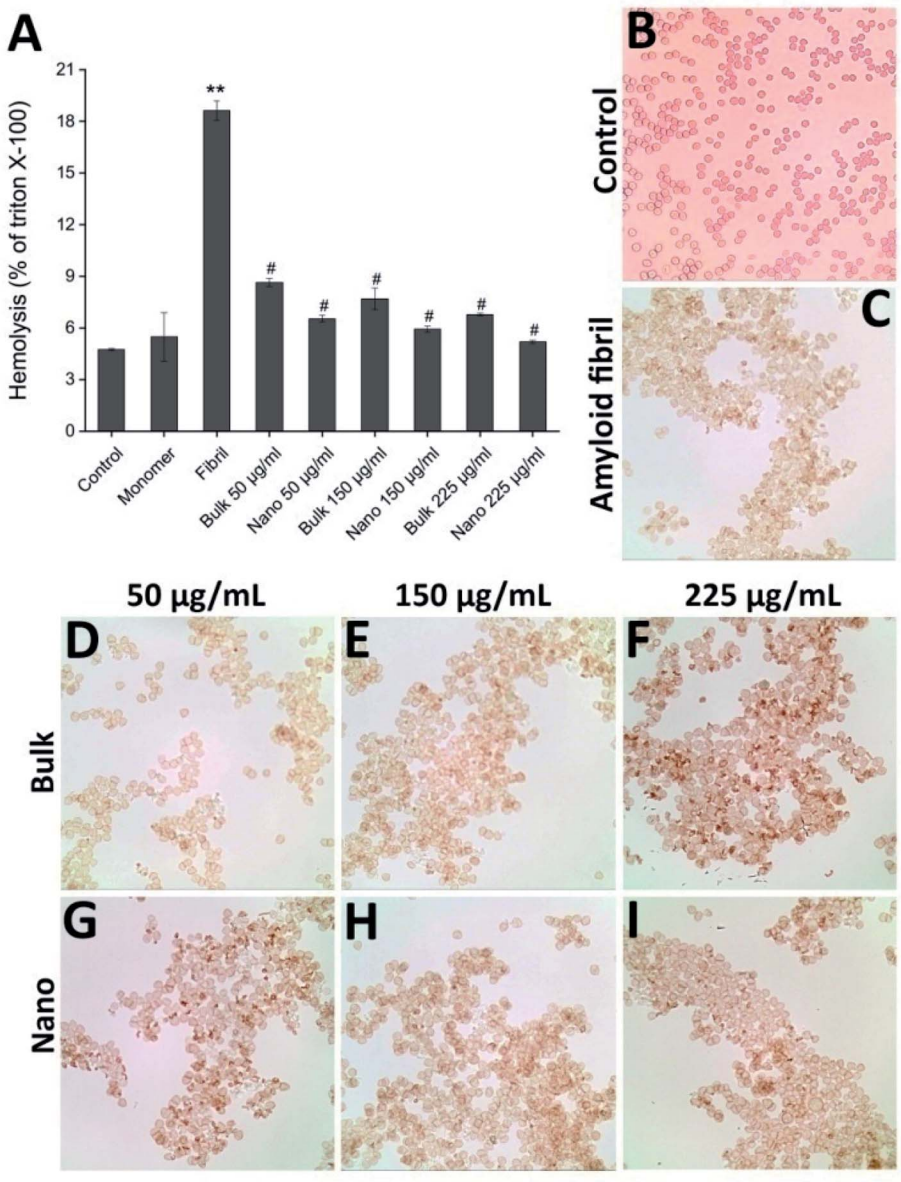

Fig. 9 Effect of the bulk and nano forms of PFPS on hemolytic activity of HEWL aggregates. (A) The percentage of hemolysis as a fraction of Triton X-100. (B–I) Optical microscopy images of samples incubated with HEWL aggregates aged either alone or with different concentrations of bulk or nano forms of PFPS. Further descriptions are provided in the text. $^{**}p < 0.001$, significantly different from control erythrocytes. $^{\#}p < 0.001$, significantly different from erythrocytes exposed only to HEWL amyloid fibrils.

© 2022 The Author(s). Published by the Royal Society of Chemistry

Open Access Article. Published on 21 March 2022. Downloaded on 6/3/2026 11:06:32 PM.
This article is licensed under a Creative Commons Attribution-NonCommercial 3.0 Unported Licence.

Effect of bulk and nano forms of PFPS on cytotoxicity and hemolytic activity of HEWL amyloid fibrils

The protective effect of PFPS nanosheets, in comparison with the respective bulk form, on toxicity of HEWL aggregates was evaluated using MTT-based cell viability and hemolysis assays. The non-toxic doses of bulk/nano forms of PFPS were determined based on the viability of SH-SY5Y human neuroblastoma cells. We found slight, if any, toxicity in relation to the bulk form of PFPS when applied at very high concentrations; whereas PFPS nanosheets were totally nontoxic (Fig. S8†). Results clearly show that HEWL fibrils, dose-dependently, reduce the cell viability (Fig. S9†). While a dose-dependent decrease in HEWL fibril-induced cytotoxicity was observed in the samples treated with either bulk or nano forms of PFPS, those containing PFPS nanosheets showed more significant viability (~73%, compared to 37%, increase in the cell viability of samples containing 225 μg mL^{-1} nano or bulk forms of PFP, respectively) (Fig. 8), indicating that substantial inhibition of HEWL fibrillation process correlates with reduced cellular toxicity. These protective effects were further corroborated by hemolysis assay. First, the effect of bulk/nano forms of PFPS on the integrity of erythrocytes membrane was investigated. We observed some permeabilization of erythrocytes membrane relating to PFPS nanosheets, when applied at high concentrations (Fig. S10†), indicating higher membrane binding capacity of nano PFPS correlates with their increased surface area. Similar to cell toxicity, a dose-dependent release of hemoglobin was observed upon treatment with HEWL amyloid fibrils of erythrocytes (Fig. S11†). This was accompanied with substantial aggregation at high concentration (Fig. S11,† inset), in accord with a previous report.[53] In the samples containing either bulk or nano forms of PFPS, however, a dose-dependent decrease in HEWL fibril-induced hemolysis was observed; where those containing nano form of PFPS were more protective (~72%, compared to 63%, decrease in the hemolysis rate of samples containing 225 μg mL^{-1} nano or bulk forms of PFP, respectively) (Fig. 9A). Interestingly, neither bulk nor nano forms of PFPS were effective in preventing erythrocytes aggregation induced by HEWL aggregates (Fig. 9D–I), suggesting that membrane aggregation does not necessarily lead to permeabilization. Altogether, obtained data indicates that PFPS nanosheets, in comparison with the respective bulk form, can more effectively mitigate fibrillation and disaggregate preformed fibrils of HEWL and related toxicity. This is proposed to occur by interfering with the initial steps of fibrillation process and constraining the protein in a native-like state with significantly buried hydrophobic regions.

Conclusion

In the present study, we demonstrated that nano form of PFPS is much more effective than the respective bulk form of PFPS in modulating fibrillation process, as well as clearance of preformed fibrils of HEWL. The obtained results suggest that delay in initiation of amyloid fibril assembly, likely due to increased water solubility and surface area upon undergoing nanonization process, is the mechanism by which PFPS nanosheets modulate amyloid fibrillation of HEWL. While there are many reports describing the effects of polyphenol-based nanoparticles on assembly process of various peptides and proteins,[9,11,54,55] we believe that our work has characteristics that distinguish it from the others. First, to avoid the profound challenges introduced by foreign additives including metals and polymers (commonly used as core materials for preparation of polyphenolic nanoparticles),[56–59] we employed direct pyrolysis to self-polymerize PFPS. Second, the PFPS nanosheets are water-soluble nano-sized particles (without limitations such as poor water solubility and low bioavailability that greatly restrict therapeutic application of natural polyphenols), and compared to the bulk form, show considerable capacity to prevent assembly process of HEWL, as at PFPS nanosheets:HEWL molar ratios of as low as 1 : 33 the fibril formation process was completely inhibited. Beside these, our preliminary experiments showed the potential of these nanosheets to use as imaging probe for detection and targeting intracellular protein aggregates. While further investigations are needed to validate these results, we suggest that polyphenol-based nanosheets have the potency to use as a straightforward strategy to design potent inhibitor relating to amyloid-related diseases.

Author contributions

A.-A. M. supervised the project, N. N. supervised preparation and characterization of the bulk and nano forms of PFPS; A.-A. M. and N. N. designed the experiments and analyzed obtained data; V. H. and A.-A. M. conducted experiments; A.-A. M., N. N., and A. M. wrote the manuscript; all authors read the manuscript and commented on it.

Conflicts of interest

The authors declare that they have no conflict of interest.

Acknowledgements

This work was supported by grants from the Research Council of the Institute for Advanced Studies in Basic Sciences (IASBS), Zanjan, Iran. The authors thank the departments of chemistry and physics of the IASBS for their valuable instrumental support.

References

1 Y. Porat, A. Abramowitz and E. Gazit, *Chem. Biol. Drug Des.*, 2006, **67**, 27–37.
2 J. Chen, H. Lin and M. Hu, *J. Pharmacol. Exp. Ther.*, 2003, **304**, 1228–1235.
3 M. Singh, M. Arseneault, T. Sanderson, V. Murthy and C. Ramassamy, *J. Agric. Food Chem.*, 2008, **56**, 4855–4873.
4 C. Tan, X. Cao, X. J. Wu, Q. He, J. Yang, X. Zhang, *et al.*, *Chem. Rev.*, 2017, **117**, 6225–6331.
5 C. Tan and H. Zhang, *Chem. Soc. Rev.*, 2015, **44**, 2713–2731.
6 F. L. O. Da Silva, M. B. D. F. Marques, K. C. Kato and G. Carneiro, *Expet Opin. Drug Discov.*, 2020, **15**, 853–864.

Open Access Article. Published on 21 March 2022. Downloaded on 6/3/2026 11:06:32 PM. This article is licensed under a Creative Commons Attribution-NonCommercial 3.0 Unported Licence.

7 H. Chen, C. Khemtong, X. Yang, X. Chang and J. Gao, *Drug Discov. Today*, 2011, **16**, 354–360.
8 K. Riehemann, S. W. Schneider, T. A. Luger, B. Godin, M. Ferrari and H. Fuchs, Nanomedicine—challenge and perspectives, *Angew. Chem., Int. Ed. Engl.*, 2009, **48**, 872–897.
9 K. Debnath, S. Shekhar, V. Kumar, N. R. Jana and N. R. Jana, *ACS Appl. Mater. Interfaces*, 2016, **8**, 20309–20318.
10 Y. Zhao, J. Cai, Z. Liu, Y. Li, C. Zheng, Y. Zheng, *et al.*, *Nano Lett.*, 2019, **19**, 674–683.
11 H. Mohammad-Beigi, D. Morshedi, S. A. Shojaosadati, J. N. Pedersen, A. T. Marvian, F. Aliakbari, *et al.*, *RSC Adv.*, 2016, **6**, 85312–85323.
12 B. Yang, Y. Dong, F. Wang and Y. Zhang, *Molecules*, 2020, **25**, 4613.
13 S. Z. Moradi, S. Momtaz, Z. Bayrami, M. H. Farzaei and M. Abdollahi, *Front. Bioeng. Biotechnol.*, 2020, **8**, 238.
14 S. Sreekumar, H. Sithul, P. Muraleedharan, J. M. Azeez and S. Sreeharshan, *BioMed Res. Int.*, 2014, **2014**, 686921.
15 D. Wang, C. Özen, I. M. Abu-Reidah, S. Chigurupati, J. K. Patra, J. O. Horbanczuk, *et al.*, *Front. Pharmacol.*, 2018, **9**, 544.
16 Y. Khajebishak, L. Payahoo, M. Alivand and B. Alipour, *J. Cell. Physiol.*, 2019, **234**, 2112–2120.
17 J. S. Jurenka, *Altern. Med. Rev.*, 2008, **13**, 128–144.
18 S. J. Choi, J. H. Lee, H. J. Heo, H. Y. Cho, H. K. Kim, C. J. Kim, *et al.*, *J. Med. Food*, 2011, **14**, 695–701.
19 S. Subash, N. Braidy, M. M. Essa, A. B. Zayana, V. Ragini, S. Al-Adawi, *et al.*, *Nutrition*, 2015, **31**, 223–229.
20 L. Rojanathammanee, K. L. Puig and C. K. Combs, *J. Nutr.*, 2013, **143**, 597–605.
21 R. E. Hartman, A. Shah, A. M. Fagan, K. E. Schwetye, M. Parsadanian, R. N. Schulman, *et al.*, *Neurobiol. Dis.*, 2006, **24**, 506–515.
22 N. Braidy, M. M. Essa, A. Poljak, S. Selvaraju, S. Al-Adawi, T. Manivasagm, *et al.*, *Oncotarget*, 2016, **7**, 64589.
23 M. M. Essa, S. Subash, M. Akbar, S. Al-Adawi and G. J. Guillemin, *PLoS One*, 2015, **10**, e0120964.
24 M. Kujawska, M. Jourdes, M. Kurpik, M. Szulc, M. Szaefer, P. Chmielarz, *et al.*, *Int. J. Mol. Sci.*, 2019, **21**, 202.
25 V. Tapias, J. R. Cannon and J. T. Greenamyre, *Neurobiol. Aging*, 2014, **35**, 1162–1176.
26 M. C. Morzelle, J. M. Salgado, M. Telles, D. Mourelle, P. Bachiega, H. S. Buck, *et al.*, *PLoS One*, 2016, **11**, e0166123.
27 M. Mizrahi, Y. Friedman-Levi, L. Larush, K. Frid, O. Binyamin, D. Dori, *et al.*, *Nanomed.: Nanotechnol. Biol. Med.*, 2014, **10**, 1353–1363.
28 M. S. Almuhayawi, W. S. Ramadan, S. Harakeh, S. K. Al Jaouni, D. J. Bharali, S. A. Mousa, *et al.*, *Saudi J. Biol. Sci.*, 2020, **27**, 1710–1716.
29 M. Ramezani, M. D. Hesami, Y. Rafiei, E. R. Ghareghozloo, A. A. Meratan and N. Nikfarjam, *ACS Appl. Bio Mater.*, 2021, **4**, 3547–3560.
30 M. R. Krebs, D. K. Wilkins, E. W. Chung, M. C. Pitkeathly, A. K. Chamberlain, J. Zurdo, *et al.*, *J. Mol. Biol.*, 2000, **300**, 541–549.
31 M. B. Pepys, P. N. Hawkins, D. R. Booth, D. M. Vigushin, G. A. Tennent, A. K. Soutar, *et al.*, *Nature*, 1993, **362**, 553–557.
32 L. Nielsen, R. Khurana, A. Coats, S. Frokjaer, J. Brange, S. Vyas, *et al.*, *Biochemistry*, 2001, **40**, 6036–6046.
33 W. E. Klunk, J. W. Pettegrew and D. J. Abraham, *J. Histochem. Cytochem.*, 1989, **37**, 1273–1281.
34 B. Katebi, M. Mahdavimehr, A. A. Meratan, A. Ghasemi and M. Nemat-Gorgani, *Arch. Biochem. Biophys.*, 2018, **659**, 22–32.
35 J. S. Kim, *Bioresour. Technol.*, 2015, **178**, 90–98.
36 G. H. Chio, M. G. Nam, S. J. Kwak, S. H. Kim, H. Chang, C. S. Shin, *et al.*, *Energy Environ. Sci.*, 2021, **14**, 3203–3215.
37 M. Altarawneh, B. Z. Dlugogorski, E. M. Kennedy and J. C. Mackie, *Prog. Energy Combust. Sci.*, 2009, **35**, 245–274.
38 R. Janoschek and W. M. F. Fabian, *J. Mol. Struct.*, 2003, **661–662**, 635–645.
39 K. R. Markham and T. J. Mabry, in *The flavonoids*, Springer, Boston, MA, 1975, pp. 45–77.
40 X. Tang, H. Yu, B. Bui, L. Wang, C. Xing, S. Wang, *et al.*, *Bioact. Mater.*, 2020, **6**, 1541–1554.
41 Y. P. Sun, B. Zhou, Y. Lin, W. Wang, K. S. Fernando, P. Pathak, *et al.*, *J. Am. Chem. Soc.*, 2006, **128**, 7756–7757.
42 H. Ding, S. B. Yu, J. S. Wei and H. M. Xiong, *ACS Nano*, 2016, **10**, 484–491.
43 P. Zhu, K. Tan, Q. Chen, J. Xiong and L. Gao, *Chem. Mater.*, 2019, **31**, 4732–4742.
44 C. Petit, M. Seredych and T. J. Bandosz, *J. Mater. Chem.*, 2009, **19**, 9176–9185.
45 C. Botas, P. Álvarez, C. Blanco, R. Santamaría, M. Granda, P. Ares, *et al.*, *Carbon*, 2012, **50**, 275–282.
46 H. He, J. Klinowski, M. Forster and A. Lerf, *Chem. Phys. Lett.*, 1998, **287**, 53–56.
47 F. Liu, M. H. Jang, H. D. Ha, J. H. Kim, Y. H. Cho and T. S. Seo, *Adv. Mater.*, 2014, **25**, 3657–3662.
48 S. Hassanzadeh, K. H. Adolfsson and M. Hakkarainen, *RSC Adv.*, 2015, **5**, 57425–57432.
49 T. Carballo, M. V. Gil, X. Gómez, F. González-Andrés and A. Morán, *Biodegradation*, 2008, **19**, 815–830.
50 J. Wang, Y. Cao, Q. Li, L. Liu and M. Dong, *Chem.–Eur. J.*, 2015, **21**, 9632–9637.
51 T. Cedervall, I. Lynch, S. Lindman, T. Berggård, E. Thulin, H. Nilsson, *et al.*, *Proc. Natl. Acad. Sci. U. S. A.*, 2007, **104**, 2050–2055.
52 S. Linse, C. Cabaleiro-Lago, W. F. Xue, I. Lynch, S. Lindman, E. Thulin, *et al.*, *Proc. Natl. Acad. Sci. U. S. A.*, 2007, **104**, 8691–8696.
53 B. Huang, J. He, J. Ren, X. Y. Yan and C. M. Zeng, *Biochemistry*, 2009, **48**, 5794–5800.
54 S. Palmal, A. R. Maity, B. K. Singh, S. Basu, N. R. Jana and N. R. Jana, *Chem. - Eur. J.*, 2014, **20**, 6184–6191.
55 A. Basu, S. Kundu, A. Das, C. Basu, S. Bhayye, S. Das, *et al.*, *Mater. Adv.*, 2020, **1**, 1142–1150.
56 N. Swilam and K. A. Nematallah, *Sci. Rep.*, 2020, **10**, 1–11.
57 M. C. Moulton, L. K. Braydich-Stolle, M. N. Nadagouda, S. Kunzelman, S. M. Hussain and R. S. Varma, *Nanoscale*, 2010, **2**, 763–770.
58 J. Liang, F. Li, Y. Fang, W. Yang, X. An, L. Zhao, *et al.*, *Colloids Surf., B*, 2011, **82**, 297–301.
59 R. Indiarto, L. P. A. Indriana, R. Andoyo, E. Subroto and B. Nurhadi, *Eur. Food Res. Technol.*, 2022, **248**, 1–24.

© 2022 The Author(s). Published by the Royal Society of Chemistry